Polytypism and band alignment in ZnSe nanowires revealed by photoluminescence spectroscopy of embedded (Zn,Cd)Se quantum dots

S. Bieker, R. Pfeuffer, T. Kiessling,[*] N. Tarakina, C. Schumacher, W. Ossau, and L. W. Molenkamp

Physikalisches Institut (EP3) der Universität Würzburg, 97074 Würzburg, Germany

G. Karczewski

Institute of Physics, Polish Academy of Sciences, Warsaw 02-668, Poland

We report on the optical characterization of single (Zn,Cd)Se quantum dots (QDs) embedded in vapor-liquid-solid-grown ZnSe nanowires (NWs). The temperature dependent quenching of the QD luminescence demonstrates that their electronic structure is comparable to that of self-assembled (Zn,Cd)Se QDs in ZnSe matrices. The photoluminescence excitation (PLE) spectrum of single nanowire QDs reveals the presence of both zinc blende (ZB) and wurtzite (WZ) crystal modifications of ZnSe in the NW shafts. PLE provides, therefore, a complementary technique to transmission electron microscopy imaging to reveal polytypism in ZnSe NWs. A transient quenching of the PL emission suggests a type II staggered band alignment at the ZB/WZ interface in our ZnSe NWs.

I. INTRODUCTION

Semiconductor nanowires are currently among the most active research fields in nanoscience. The vapor-liquid-solid (VLS) growth mode [1] enables the self-assembled growth of nanowires (NWs) with nm-sized diameters at lengths in excess of several μm and is applicable to a large variety of material systems. Only recently, successful incorporation of optically active (Zn,Cd)Se quantum dots into ZnSe NWs has been demonstrated [2]. The embedded quantum dots (QDs) show single photon emission up to 220 K [3] and are thus a promising candidate for spectrally narrow single photon sources at room temperature.

However, the widely observed polytypism in ZnSe NWs accompanied by a high density of stacking faults is a major obstacle for the performance of NW-based optical devices [4]. Transmission electron microscopy (TEM) imaging is widely applied as the method of choice to gain insight into the crystal structure of single NWs [5,6]. In this paper, we demonstrate that photoluminescence excitation spectroscopy is also capable of providing information on the presence of different crystalline modifications in single NWs. To bypass the poor photoluminescence (PL) emission from pure polytypic ZnSe NWs, we incorporate single (Zn,Cd)Se QDs in the wires, which due to rapid carrier capture and good optical properties then serve as an all-optical probe of their crystalline environment. From the excitation spectrum we can extract information on the crystalline composition of the NWs. Furthermore, we observe a time-resolved quenching of the QD luminescence, which suggests a type II staggered band alignment at the interface of the wurtzite/zinc blende (WZ/ZB) domains in our polytypic NWs. Photoluminescence excitation (PLE) and time-resolved PL provide, therefore, complementary techniques to conventional TEM imaging to assess the crystal structure of semiconductor NWs.

II. SAMPLE GROWTH AND EXPERIMENTAL SETUP

The NWs are grown on $\langle 001 \rangle$-oriented GaAs:Si substrates in a molecular beam epitaxy (MBE) chamber in the VLS growth mode. The chamber is equipped with evaporation cells of elemental Zn, Se, and Cd as source materials. Prior to the NW growth, the substrate is thermally deoxidized at 640°C under UHV conditions. A 1 nm Au layer is deposited in a connected electron beam evaporation chamber and heated up to 500°C for 10 min. Dewetting of the Au layer results in the formation of Au-Ga eutectic droplets serving as the catalyst for the subsequent NW growth. The substrate temperature is reduced and stabilized at the growth temperature of 400°C. The growth process is initiated by exposing the seed droplets to the molecular beams of the NW constituents Zn and Se. Growth is carried out under Se rich conditions with a Se:Zn (Se:Cd) flux ratio of 2:1 (3:1) and a beam equivalent pressure on the order of 1×10^{-7} T. Switching the Zn flux to a Cd flux for 20 s after 50 min of growth time introduces the (Zn,Cd)Se inclusion into the NW body. Switching back to Zn flux for 10 min finalizes the growth process. A second sample without the (Zn,Cd)Se inclusion is fabricated as a reference sample.

A scanning electron microscopy (SEM) image of the as-grown NW sample with a (Zn,Cd)Se QD is displayed in Fig. 1(a). The wires have typical diameters of 10 to 15 nm and a mean length of 1 μm. No overall ordering in the growth direction of the NWs is observed. Droplets of the Au catalyst remain on the tip of most of the wires.

For the μ-PL characterization of single NWs, the wires are mechanically dispersed on clean, nonemitting Si substrates. SEM imaging reveals regions on the new host substrate with spatially isolated single NWs [Fig. 1(b)] or small clusters of few NWs that stick together. The small areal density of the transferred NWs allows one to address individual wires by means of our focusing optics and to study the PL emission of single NW QDs. The sample is, therefore, mounted on the coldfinger of a liquid helium flow optical cryostat. Tunable optical excitation is provided by a Stilbene-3 charged dye laser pumped by an Ar$^+$ laser, the output power of which

---

[*]tobias.kiessling@physik.uni-wuerzburg.de
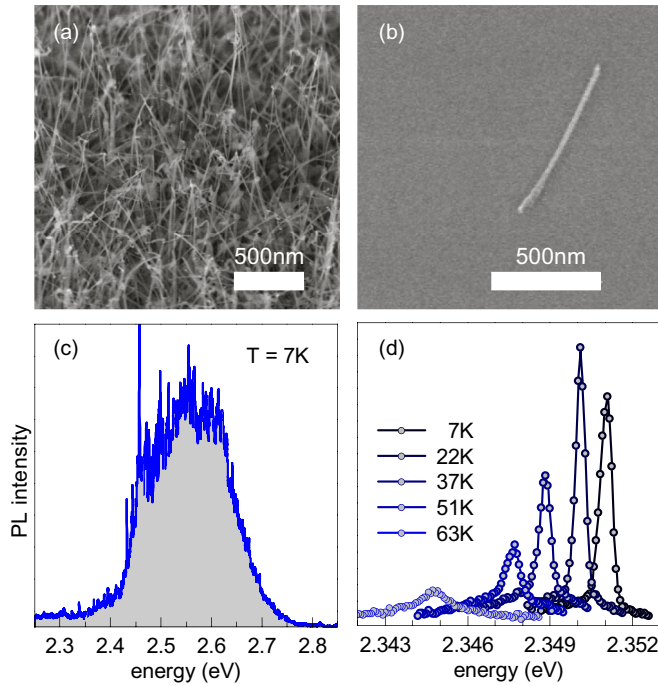
FIG. 1. (Color online) SEM images of (a) the as-grown NW sample with embedded QDs and (b) a single NW dispersed on a clean Si substrate. (c) PL spectrum of the as-grown wafer. The sharp lines originate from radiative decay of (multi)excitons localized in embedded single (Zn,Cd)Se QDs. (d) Temperature evolution of the emission spectrum of a single QD embedded in a single NW. Note that the emission intensity at 22 K is increased over the low-temperature emission at 7 K.

is stabilized to within 1% accuracy by a liquid crystal laser stabilizer. Luminescence is collected in a confocal geometry by a 0.4 numerical aperture microscope objective, spectrally dispersed in a 1 m focal length monochromator equipped with a $1200\,\mathrm{mm}^{-1}$ grating, and detected by a liquid nitrogen cooled charge-coupled device (CCD) array.

The TEM study has been carried out using a FEI Titan 80-300 (S)TEM operated at 300 kV and equipped with an EDAX energy dispersive X-ray (EDX) microanalysis detector. For the TEM study, wires were distributed on a holey carbon film supported on a Cu grid by gentle scraping of the substrate wafer.

III. OPTICAL CHARACTERIZATION OF SINGLE EMBEDDED QDs

A PL spectrum of the as-grown wafer is reported in Fig. 1(c). At focused optical excitation, the spectrum decomposes into an energetically broad ensemble of sharp PL lines. We show in the following that these optical transitions are not related to impurities or excitons localized at structural defects, such as the WZ/ZB junction [4,7], but originate from the radiative decay of neutral or charged (multi)excitons in individual (Zn,Cd)Se QDs. We, therefore, study the excitation density and lattice temperature dependence of the emission intensity of such single PL lines.
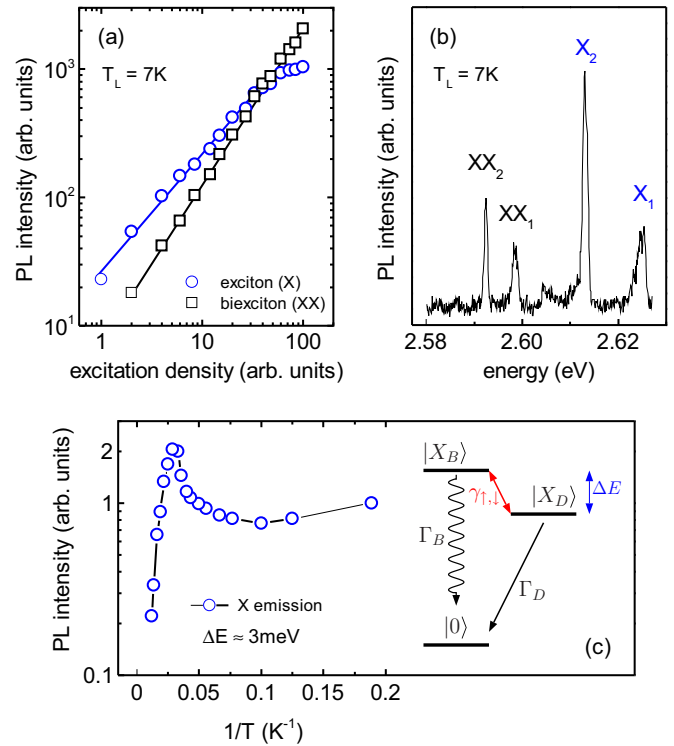
FIG. 2. (Color online) From the excitation density dependence of single emission lines (a), each line in the μ-PL spectrum (b) can be assigned to the radiative decay of neutral excitons (Xs) or biexcitons (XXs). Transitions with the same numerical index belong to the same QD. (c) Temperature induced quenching of the PL emission intensity of a single QD exciton. The increase of the PL intensity at moderate sample temperatures indicates the thermally activated repopulation of bright exciton states $|X_B\rangle$ from the dark exciton ground state $|X_D\rangle$.

Depending on the number of NWs that reside within the laser focus, a typical low-power μ-PL spectrum of a sample with dispersed wires consists of only one or a few emission lines. Upon increasing the excitation power, additional lines appear on the low-energy side of the spectrum. This behavior is characteristic of QD emission where the low-energy PL lines originate from the radiative decay of biexcitons. Emission lines that scale linearly with excitation power [cf. Fig. 2(a)] identify neutral exciton (X) luminescence. Larger scaling exponents [1.22 ± 0.02 for black markers in Fig. 2(a)] reveal charged exciton (CX) or biexciton (XX) emission. Due to the different power laws and as a consequence of the dark exciton ground state in the QD energy level scheme [cf. Fig. 2(c)], biexciton luminescence dominates over neutral exciton emission at large excitation densities [8] and identifies the low-energy PL lines in Fig. 2(b) as XX. The biexciton binding energy of $\approx 20\,\mu$eV, which we observe in our samples, is typical for both self-assembled [9,10] and NW-based (Zn,Cd)Se QDs [8,11] and further corroborates our XX assignment.

We show in Fig. 1(d) the temperature dependent X emission of a single QD, which exhibits a marked redshift and a typical line broadening from $500\,\mu$eV to 1.5 meV full width at half maximum (FWHM) as the sample temperature T_L increases from 7 to 60 K. This behavior is familiar from self-assembled single QDs. The redshift is induced by the temperature

evolution of the barrier and QD material's fundamental band gap and the broadening originates from enhanced interaction with acoustic phonons [12]. We observe on all investigated single PL lines that the emitted PL intensity reaches a maximum at moderate sample temperatures, i.e., the PL emission does not decline monotonically as a function of T_L. This distinct temperature dependence, which is shown in detail for a representative X emission line in Fig. 2(c), is closely related to the QD energy level scheme. The electron-hole exchange interaction splits the QD exciton state into an optically active (bright) state $|X_B\rangle$ with angular momentum $J_z = \pm 1$ and a dark energetic ground state $|X_D\rangle$ with $J_z = \pm 2$ [cf. Fig. 2(c)] [9,13]. At low sample temperatures, only bright excitons contribute to PL emission, while momentum conservation protects the dark states against radiative decay. When the thermal energy $k_B T$ becomes comparable to the bright-dark energetic splitting ΔE, dark excitons are thermally activated to the bright state and contribute then to PL emission. We observe this repopulation in Fig. 2(c) by the maximum of the emitted PL intensity at ≈ 35 K, from which we estimate $\Delta E \approx 3$ meV. This value is in good agreement with previously reported bright-dark splittings in NW-based (Zn,Cd)Se QDs [11].

Both the excitation density and sample temperature dependence of the emission properties demonstrate unambiguously the QD origin of the sharp emission lines in the PL spectra of our NW samples.

IV. POLYTYPISM AND BAND ALIGNMENT IN THE ZnSe NW BODY

A typical TEM image of a single pure ZnSe NW (reference sample) is displayed in Fig. 3(a). Domains with both ZB and WZ modifications of ZnSe in the NW body are observed. Our data are in line with the results obtained from previous TEM studies of NWs of several different material combinations [2,5,6,14]. TEM experiments performed on the NWs with embedded QDs also show a high concentration of stacking faults in the wires. Imaging of these very thin NWs, however, is significantly complicated by charging of the wires, which leads to the wire vibrating on the support carbon film and difficulties with direct visualization of the QDs. An impediment towards direct imaging of the embedded QDs is the gradual change in the chemical composition of the ternary (Zn,Cd)Se inclusions, which makes direct Z-contrast imaging of the QD challenging. Energy filtered transmission electron microscopy (EFTEM) can be used to visualize the embedded QDs in single NWs [5]. However, such experiments are difficult to perform on a daily basis. While TEM is a powerful tool to directly image the crystal structure of single NWs, we show in the following that PLE spectroscopy of embedded QDs is a fast and easy characterization technique that also reveals the polytypic crystal structure of single NWs. Being an all-optical method, PLE is also applicable to very thin NWs on which we find TEM imaging to be aggravated by charging and vibrating of the object.

For PLE measurements, the excitation wavelength of the dye laser is tuned from 4590 to 4300 Å in steps of 0.25 Å. At each wavelength, a full CCD spectrum is recorded. We show in Fig. 4(a) a representative PL/PLE map where horizontal
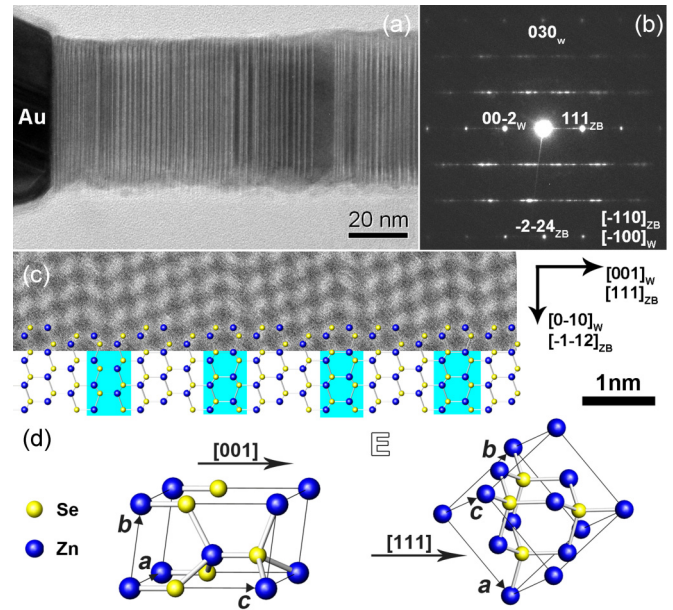
FIG. 3. (Color online) (a) TEM image of a single ZnSe NW, showing a high concentration of stacking faults. The seed droplet of the Au-Ga catalyst is located on top of the wire. Note the presence of an amorphous shell around the droplet. (b) Selected-area electron diffraction (SAED) pattern obtained from the wire; indexing in ZB and WZ lattices is shown. The distribution of the spots on the SAED pattern suggests that the wire mainly can be described as a ZB twinned wire grown along the $\langle 111 \rangle$ direction. Both ZB and WZ domains are different in size along the length of the wire (no periodical domain structure is present), resulting in the appearance of diffuse streaks in the SAED pattern. (c) High-angle annular dark-field scanning transmission electron microscopy image partly overlapped with a sketch of the crystal structure of the wire, showing a distribution of ZB (white background) and WZ (blue background) domains. (d) and (e) are sketches of wurtzite and zinc blende unit cells of ZnSe.

line cuts yield PL spectra at a fixed excitation wavelength and vertical line cuts yield excitation spectra at a given detection energy. Analysis of the spectral diffusion [10] (not shown here) demonstrates that both PL lines originate from two separate QDs.

Due to the small absorption volume of a single QD, we detect no PL emission for excitation energies considerably below the 1s exciton state $E_{X,ZB}$ in cubic ZnSe at 2.80 eV [15]. As the excitation wavelength is tuned to higher excitation energies, a broad resonance in the QD PL intensity is observed at the fundamental band gap of cubic ZnSe at $E_{g,ZB} = 2.82$ eV. A second resonance is seen at the 2.87 eV excitation energy, which we assign to the band gap [16] of the hexagonal ZnSe modification $E_{g,WZ} = 2.874$ eV [17]. The observation of absorption signatures from both hexagonal and cubic modifications of ZnSe is in nice agreement with the presence of alternating WZ and ZB domains in the NWs revealed in the TEM image (cf. Fig. 3). Our results corroborate the usefulness of PLE spectroscopy as a complementary technique to TEM imaging for the crystal structure analysis of semiconductor NWs [18–21].

Interestingly, the resonances in the PL emission from our NW QDs are detected at the band gaps of the WZ and
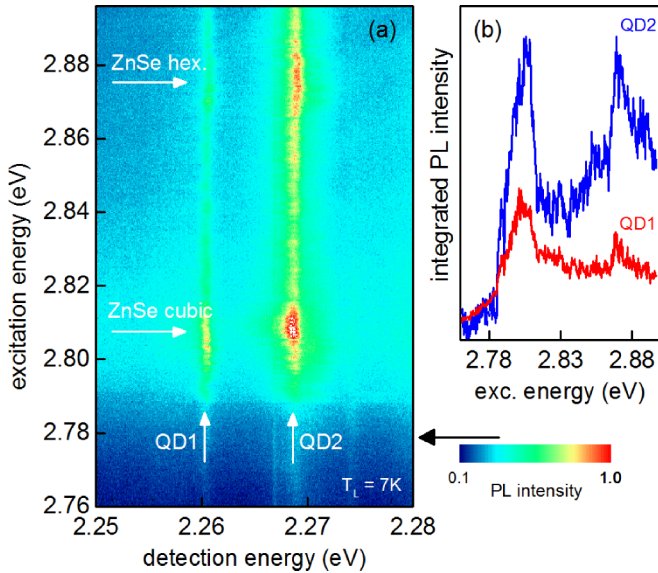
FIG. 4. (Color online) (a) PL/PLE map of two single (Zn,Cd)Se QDs embedded in two distinct ZnSe NWs. Resonances in the emission intensity are detected at excitation energies equal to the fundamental band gaps of the ZB and WZ modification of ZnSe. (b) Integrated PL intensities [arbitrary (arb.) units] of both QDs as a function of the excitation energy.

FIG. 5. (Color online) Quenching of the PL emission from our as-grown NW-based QDs. Above-band gap cw optical excitation is switched on at 0 s delay. (a) The nonexponential transient PL quenching and its marked excitation density dependence suggest a charging process in the NWs. (b) At increasing sample temperatures, carriers are thermally activated out of the QDs and are trapped at the WZ/ZB interface with staggered type II band alignment. This space charge leads to a band bending and to a depletion of the QDs.

ZB modifications of *bulk* ZnSe. The reason, therefore, is twofold. Previous studies have shown from the analysis of conceptual Kronig-Penney models [22] that the admixture of WZ segments in a predominantly ZB NW body with a type II staggered band alignment at the WZ/ZB interfaces eventually leads to a redshift of the fundamental PL transitions [23]. This redshift might counter a blueshift due to radial carrier confinement in our very thin NWs. On the other hand, small residual deviations from the bulk absorption edges are masked by the ≈ 20 meV width of the PLE absorption peaks in our experiment. We note that in previous studies, i.e., on highly polytypic InP NWs [14], PL was detected at the energetic position of the bulk ZB InP band gap, which is consistent with our observation of the bulk ZB/WZ absorption edges in the PLE spectrum.

We observe a time-dependent quenching of the QD PL in our polytypic ZnSe NWs under cw optical excitation, which is summarized in Fig. 5. Here we show the total, spectrally integrated PL emission from the as-grown NW ensemble. Maximum PL emission is recorded when the cw laser source is switched on at 0 s delay. As time elapses, the PL intensity decreases nonexponentially and saturates after sufficiently long delays. A faster quenching is seen at increased excitation densities. Together with the comparably slow timescale of the quenching, these observations suggest a charging process somewhere in the NWs. We note that neither thermal cycling nor interruption of the laser excitation leads to a recovering of the PL intensity.

Mere structural damage in the sample (i.e., burning of the NWs) due to laser heating is ruled out as an explanation for the quenching by the variation of the excitation wavelength. We, therefore, tune λ_{exc} below the ZnSe fundamental band gap at 2.80 eV and illuminate the sample for several minutes at high

excitation density. After that treatment, the identical absolute PL intensity and time-dependent quenching upon above-band gap excitation is detected as for the case without previous below-band gap illumination.

The observed PL quenching in our polytypic ZnSe NWs suggests a type II band alignment at the WZ/ZB interface, which was previously predicted for bulk ZnSe [24] and was reported for polytypic NWs of different compound semiconductors [14,25]. Due to the few nm thin randomly alternating WZ and ZB domains in our highly polytypic NWs, the electron and hole wave functions are delocalized along the wire axis and not confined to such single domains. The spatial concentration of the electron and hole wave functions can, however, be displaced in the axial direction: electrons are concentrated in ZB-rich regions of the NW body, and holes are concentrated in WZ-rich regions [14]. In our experiment, above-band gap optical excitation creates free charge carriers, which are eventually captured by the embedded QDs and contribute then to PL emission. A competing mechanism, however, is the spatial separation of electrons and holes due to the axially displaced concentration of their wave functions. This situation only occurs in a polytypic structure with a staggered type II band alignment and suppresses the radiative recombination of the photocarriers. The accumulative charging of the NWs leads to a band bending and ultimately to a depletion of the embedded QDs such that these wires turn dark and do no longer contribute to the PL spectrum.

We observe no spectral shift or transformation of the overall PL spectrum during the charging (PL quenching) process. Size and composition fluctuations among the QD ensemble, which lead to the inhomogeneous broadening of the PL emission band in Fig. 1(c), are not correlated with the charging affinity of individual wires. We note that the excitation density, excitation wavelength, and lattice temperature dependence of the PL quenching corroborate our charging interpretation. Increased excitation density provides more free band carriers, which accelerates the charging process [cf. Fig. 5(a)]. Below-band

gap optical excitation does not lead to a charging of the NWs and hence no quenching of the PL emission is observed. At elevated sample temperatures, charge carriers are thermally activated out of the QDs and are spatially displaced along the NW axis. This accumulative charging leads to a progressive reduction of the PL saturation level as displayed in Fig. 5(b).

V. SUMMARY AND CONCLUSION

To conclude, we have fabricated self-assembled ZnSe NWs in the VLS-growth mode with embedded optically active (Zn,Cd)Se QDs. We have shown that the PL emission from our NWs is due to the embedded QDs and that their energetic structure is comparable to that of conventional self-assembled

QDs. We have demonstrated that the QD PL can be used as an all-optical probe of the crystalline environment in the NW shafts. The excitation spectrum reveals the presence of both ZB and WZ modifications of ZnSe, which is in line with the polytypic crystal structure seen in TEM imaging. From a transient quenching of the QD luminescence we infer a staggered type II band alignment at the WZ/ZB interface in our polytypic ZnSe NWs.

[1] R. S. Wagner and W. C. Ellis, Appl. Phys. Lett. **4**, 89 (1964).

[2] M. Den Hertog, M. Elouneg-Jamroz, E. Bellet-Amalric, S. Bounouar, C. Bougerol, R. André, Y. Genuist, J. P. Poizat, K. Kheng, and S. Tatarenko, J. Appl. Phys. **110**, 034318 (2011).

[3] A. Tribu, G. Sallen, T. Aichele, R. André, J.-P. Poizat, C. Bougerol, S. Tatarenko, and K. Kheng, Nano Lett. **8**, 4326 (2008).

[4] U. Philipose, T. Xu, S. Yang, P. Sun, H. E. Ruda, Y. Q. Wang, and K. L. Kavanagh, J. Appl. Phys. **100**, 084316 (2006).

[5] M. Den Hertog, M. Elouneg-Jamroz, E. Bellet-Amalric, S. Bounouar, C. Bougerol, R. André, Y. Genuist, J. P. Poizat, K. Kheng, and S. Tatarenko, J. Cryst. Growth **323**, 330 (2011).

[6] H. Shtrikman, R. Popovitz-Biro, A. Kretinin, L. Houben, M. Heiblum, M. Bukała, M. Galicka, R. Buczko, and P. Kacman, Nano Lett. **9**, 1506 (2009).

[7] T. Aichele, A. Tribu, C. Bougerol, K. Kheng, R. André, and S. Tatarenko, Appl. Phys. Lett. **93**, 143106 (2008).

[8] G. Sallen, A. Tribu, T. Aichele, R. André, L. Besombes, C. Bougerol, S. Tatarenko, K. Kheng, and J. P. Poizat, Phys. Rev. B **80**, 085310 (2009).

[9] G. Bacher, R. Weigand, J. Seufert, V. D. Kulakovskii, N. A. Gippius, A. Forchel, K. Leonardi, and D. Hommel, Phys. Rev. Lett. **83**, 4417 (1999).

[10] B. Patton, W. Langbein, and U. Woggon, Phys. Rev. B **68**, 125316 (2003).

[11] S. Bounouar, C. Morchutt, M. Elouneg-Jamroz, L. Besombes, R. André, E. Bellet-Amalric, C. Bougerol, M. Den Hertog, K. Kheng, S. Tatarenko, and J. Ph. Poizat, Phys. Rev. B **85**, 035428 (2012).

[12] L. Besombes, K. Kheng, L. Marsal, and H. Mariette, Phys. Rev. B **63**, 155307 (2001).

[13] M. Nirmal, D. J. Norris, M. Kuno, M. G. Bawendi, Al. L. Efros, and M. Rosen, Phys. Rev. Lett. **75**, 3728 (1995).

[14] J. Bao, D. C. Bell, F. Capasso, J. B. Wagner, T. Mårtensson, J. Trägårdh, and L. Samuelson, Nano Lett. **8**, 836 (2008).

[15] G. E. Hite, D. T. F. Marple, M. Aven, and B. Segall, Phys. Rev. **156**, 850 (1967).

[16] Due to the weaker spin-orbit coupling in ZnSe, the energetic splitting of the Γ_7/Γ_9 hole bands in WZ ZnSe is presumably significantly smaller than the related 25 meV splitting in WZ CdSe [17] and therefore masked by the $\approx$20 meV width of the PLE absorption peaks.

[17] *Semiconductors. B: II-VI and I-VII Compounds; Semimagnetic Compounds* edited by U. Rössler (Springer, Berlin, Heidelberg, New York, 1999).

[18] X. Wang, I. Zardo, D. Spirkoska, S. Yazji, K. W. Ng, W. S. Ko, C. J. Chang-Hasnain, J. J. Finley, and G. Abstreiter, ACS Nano **8**, 11440 (2014).

[19] S. Perera, K. Pemasiri, M. A. Fickenscher, H. E. Jackson, L. M. Smith, J. Yarrison-Rice, S. Paiman, Q. Gao, H. H. Tan, and C. Jagadish, Appl. Phys. Lett. **97**, 023106 (2010).

[20] P. Corfdir, B. Van Hattem, E. Uccelli, A. F. i. Morral, and R. T. Phillips, Appl. Phys. Lett. **103**, 133109 (2013).

[21] M. De Luca, G. Lavenuta, A. Polimeni, S. Rubini, V. Grillo, F. Mura, A. Miriametro, M. Capizzi, and F. Martelli, Phys. Rev. B **87**, 235304 (2013).

[22] R. d. L. Kronig and W. G. Penney, Proc. R. Soc. London, Ser. A **130**, 499 (1931).

[23] M. Heiss, S. Conesa-Boj, J. Ren, H.-H. Tseng, A. Gali, A. Rudolph, E. Uccelli, F. Peiró, J. R. Morante, D. Schuh, E. Reiger, E. Kaxiras, J. Arbiol, and A. Fontcuberta i Morral, Phys. Rev. B **83**, 045303 (2011).

[24] M. Murayama and T. Nakayama, Phys. Rev. B **49**, 4710 (1994).

[25] P. Kusch, E. Grelich, C. Somaschini, E. Luna, M. Ramsteiner, L. Geelhaar, H. Riechert, and S. Reich, Phys. Rev. B **89**, 045310 (2014).